A&A manuscript no.
(will be inserted by hand later)

Your thesaurus codes are:
08.13.2; 08.16.4; 08.03.4; 08.12.1l; 13.18.7; 02.12.3

ASTRONOMY
AND
ASTROPHYSICS
31.5.1994

Circumstellar CO emission in S stars

I. Mass-loss with little or no dust

R. Sahai[1,2,3] and S. Liechti[4]

[1] Jet Propulsion Laboratory, MS169-506, 4800 Oak Grove Dr., Pasadena, CA 91109, USA
[2] Chalmers University of Technology & Gothenburg University, Gothenburg, S-41296, Sweden
[3] Senior Resident Research Associate, National Research Council, National Academy of Sciences, Washington, DC
[4] Centro Astronómico de Yebes (IGN), Apartado 148, E-19080 Guadalajara, Spain

Received ??, Accepted May 9, 1994

Abstract.

47 S stars have been searched for circumstellar CO (J=1–0 and/or 2–1) emission, and 29 have been detected, including 4 which show no evidence of dust in their *IRAS* LRS spectra, and one with possibly no Tc (and therefore not an AGB star). Six stars show anomalous features in their profiles, showing the presence of more than one kinematic component in the expanding outflow. Two stars may have detached-shell envelopes. The mean expansion velocity distribution for S stars envelopes is different than that for C-rich stars, with the former having a slightly lower mean expansion velocity, and a significantly higher fraction of objects with very low expansion velocities ($\lesssim 5.5$ km s^{-1}). In most S stars, the mass-loss rates are $> 2\times10^{-7}$ M$_\odot$ yr^{-1} and the gas-to-dust ratios are > 1000. Our detection of CO in S stars with little or no detectable dust implies substantial mass-loss in these objects. The expansion velocities and mass-loss rates of the relatively dust-free stars show a much steeper dependence on the the far-infrared excess (ΔIR$_e$), as compared to the more dusty stars. This suggests that when the amount of dust becomes small, mass-loss may be partially driven by a different mechanism than radiation pressure on grains, which probably dominates in the dusty envelopes.

Key words: Stars: mass-loss – Stars: AGB and post-AGB – Circumstellar matter – Stars: late-type – Radio lines:molecular – Line:profiles

1. Introduction

S stars are asymptotic branch (AGB) red giants, with the unique chemical property that in their atmospheres, [O]=[C] within a factor 1.05 (Scalo & Ross 1976), making their atmospheric chemistry perhaps quite different from that of either O-rich or C-rich red giants. This property results from the dredge-up of C from shell-He burning to the stellar surface — a process that distributes red giants along a composition axis represented by the spectral types M–MS–S–SC–C. Chen & Kwok (1993) have grouped S stars into different circumstellar classes, depending on their *IRAS* LRS spectra — the 3 main classes being *class-E* (9.7 μm silicate emission feature), *class-F* (featureless dust continuum), and *class-S* (stellar photospheric spectrum). A comparison of circumstellar CO emission from the different LRS classes potentially provides a sensitive, quantitative test of how mass-loss outflow properties depend on the presence or absence of circumstellar dust. However, such a test has not been possible since very few S stars had been detected in CO emission until recently, all belonging to *class-E*. In addition, large uncertainties existed in analyses of S star mass-loss properties based on the *IRAS* far-infrared fluxes (e.g. Jura 1988), because the outflow velocities and the gas-to-dust ratios were not known. In this paper, we report the results of a search for CO emission from circumstellar envelopes (CSEs) in a sample of S stars which has resulted in the detection of mass-outflows from stars with no detectable dust in their *IRAS* LRS spectra.

Send offprint requests to: R.Sahai

2. Observations

We have searched for one or both of the CO J=1–0 and 2–1 lines in a total of 47 S stars (including MS and SC stars) selected from Stephenson's (1984) catalog with an *IRAS* 60μm flux >1 Jy, using the SEST 15-m (from 1988 August–1990 April) and the IRAM 30-m telescopes (8–10 July 1990). Coordinates have been taken from the *IRAS* Point Source catalog. The system temperatures and main-beam efficiencies respectively were about 650K and 0.74 (115GHz) and 1100K and 0.54 (230GHz) at SEST, and 1300–1900K and 0.45 at IRAM. The spectrometers used were: a) at SEST, 2 acousto-optical spectrometers (bandwidth/channel separation of 86 MHz/43 KHz, and 500 MHz/0.7 MHz), and b) at IRAM, 2 filterbanks (256 × 100 kHz and 512 × 1 MHz).

3. Results

We have detected CO emission in 29 stars and set sensitive upper limits for most of the undetected objects (typically 10–20 mK). The lines have been fitted by an empirical line-shape function described by Wannier et al. (1990), in order to derive

Table 1. Survey S stars

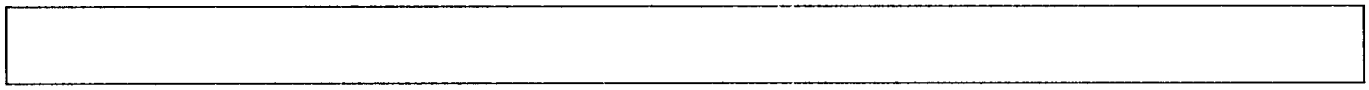

Fig. 1. CO (J=1–0 and/or 2–1) spectra of selected S (including MS and SC) stars. The spiky features seen in some spectra are due to line-of-sight interstellar emission. Anomalous features can be seen in the spectra for χ Cyg (Fig. 1p), W Aql (Fig. 1n), DK Vul (Fig. 1r), R Gem (Fig. 1c), and TT Cen (Fig. 1f). In the case of R Gem, TT Cen, W Aql, and DK Vul, spectra produced by folding the data around the line-center to improve the signal-to-noise ratio are also presented - these show the anomalous features in the line profiles more clearly

the source velocity (V_c), the expansion velocity of the CSE (V_e), the peak line intensity (T_{mb}), and the line-shape parameter, α (Table 1). Bieging & Latter (1994) have detected several objects in our sample, however the velocity resolution (2.6 km s^{-1}) and often the signal-to-noise ratios in their spectra, is generally significantly poorer than in our study and inadequate for determining expansion velocities with sufficient precision. We detect CO in DY Gem (implying a substantial mass-loss rate), one of the two (BD Cam and DY Gem) stars in our sample which are "accidental" S stars (i.e. without ^{99}Tc, and therefore not thermally-pulsing AGB stars; see Jorissen et al. 1993) and expected to have very low mass-loss rates. However, Groenewegen (1993) claims that the "non-detection" of Tc in DY Gem is uncertain. Our detection of substantial mass-loss in this object makes it very important to definitively settle the issue of whether or not DY Gem is an "accidental" S star.

3.1. Line profiles

An outstanding result from our survey has been the discovery of a very unusual, extended, asymetric outflow in the prototype S star π^1 Gru (Sahai 1992). In this object, the CO lines display weak high-velocity wings and narrow features, seen so far only in one other red giant, C-rich V Hydra (Kahane, Maizels, and Jura 1988), and probably result from the presence of a secondary, fast bipolar outflow, embedded inside a slow primary, spherical outflow (Sahai & Wannier 1988). An inspection of the line profiles in Fig. 1 (a-w) shows that anomalous features are present in the case of χ Cyg (Fig. 1p), W Aql (Fig. 1n), DK Vul (Fig. 1r), R Gem (Fig. 1c), and TT Cen (Fig. 1f). For the latter four objects, these features can be more clearly seen in the lower spectrum, where the data have been folded around the line center to increases the signal-to-noise, and reduce the effect of random irregularities in the CSE on the profiles. The line profiles in χ Cyg, W Aql, and R Gem show the presence of weak wing emission features. In DK Vul and TT Cen, the line profile is composite, with a narrow central feature, and a broader basal feature. The broad emission components indicate the presence of secondary outflow components which may be bipolar, as in V Hydra and π^1 Gru. In RZ Sgr (Fig. 1s), the J=2–1 line profile gives a significantly lower V_e compared to J=1–0. Possible explanations are that the J=2–1 emission comes from an inner outflow, or a compact, equatorially dense region (e.g. a disk), expanding more slowly than the more extended outflow seen in J=1–0 emission. The above "anomalous-line stars" are amongst the strongest CO emitters in our sample, suggesting that such anomalous features in the line-shapes may be more ubiquitously present in S stars. Margulis et al. (1990) find similar anomalous features in the CO J=1–0 spectra of a few O-rich stars.

In FU Mon, the CO line consists of two narrow ($\Delta V \approx 4$ km s^{-1}) spikes at $V_{lsr} = -42$ and 11 km s^{-1}, with very weak emission in between. Similar profiles have been found for 3 bright N-type carbon-stars (out of 65 surveyed), arising from a spatially-resolved "detached-shell" CSE structure (Olofsson, et al 1990). There is some chance that the spiky CO emission in FU Mon is interstellar (when the reference position was 11′ offset from the source, we found a narrow "absorption" interstellar feature at V_{lsr} = 3 to 10 km s^{-1}). However, we believe it to be circumstellar, since the weak emission between the spiky features, covers too broad a velocity range to be interstellar, and when we moved the reference position closer (2.′7) the individual spectra did not show the "absorption feature". The UY Cen line-profile is fitted best by a double-peaked shape (negative α). With folding the data around the line center, the line shape not only shows the narrow emission feature at the expansion velocity, but also a weaker central peak, similar to that seen in the detached-shell carbon-stars. Thus, FU Mon and UY Cen may possibly have detached-shell CSEs.

3.2. Outflow Properties

We have correlated the outflow characteristics derived from the CO spectra (expansion velocity V_e, mass-loss rate) with other stellar (period) and circumstellar (dust emission) characteristics. Seven additional S stars, not observed in our survey, but detected previously in CO emission, have been added to the sample in order to improve the statistics (Table 1, italicised source names). The star AD Cyg, from Bieging and Latter's survey (1994) was not included because the coordinates used in their observations are incorrect. The correct 1950 coordinates are $\alpha = 20^h29^m36^s.4$, $\delta = 32°23'41''$ (Plaut 1977).

3.2.1. Expansion velocity

The V_e distribution of S star CSEs shows a broad peak between 5–15 km s^{-1}, with a mean, $< V_e >$ =11.3 km s^{-1} (Fig. 2). We have compared it with the V_e distribution of a sample of bright (K mag < 2) C-rich stars (Olofsson et al. 1994). Although both samples show a similar range of expansion velocities (roughly 5 to 25 km s^{-1}), the S stars have a significantly larger fraction of low outflow velocity sources ($V_e \lesssim 5.5$ km s^{-1}): $22 \pm 8\%$ of S stars with detected outflows have small expansion velocities compared to $6 \pm 3\%$ for the C-rich stars. The 8 small-V_e stars

Fig. 2. The gas expansion velocity (V_e) distribution for S stars

Fig. 3. The gas expansion velocity (V_e) versus (a) infrared-excess (ΔIR_e), (b) variability period (P). Different symbols represent different classes based on the *IRAS* LRS spectra (as defined by Chen and Kwok 1993) – E: 9.7 μm silicate emission feature, F: featureless dust continuum, S: stellar photospheric spectrum, and C: 11.3 μm silicon carbide feature

are almost only *class-F* and *class-S* objects. Statistical tests for comparing the S star and C star V_e-distributions give (a) a 3% probability that the 2 distributions are intrinsically the same, and (b) a 19% probability that $< V_e >$ for the C-stars (12.9 km s^{-1}) is the same as for the S stars. A plot of V_e versus the infrared excess, ΔIR_e (as defined by Wannier et al. 1990) shows a strong correlation for $\Delta IR_e > 10^{-1}$, but a weak correlation for $\Delta IR_e < 10^{-1}$ (Fig. 3a). Separating our sample into different circumstellar classes, we find that for the *class-E* stars (which have the highest ΔIR_e's), there is a strong correlation between V_e and ΔIR_e, but for the *class-F* and *-S* stars (which have the lowest ΔIR_e's), the correlation is significantly weaker (or steeper, or both), with V_e taking on a large range of values for a small range of ΔIR_e. V_e also shows an increase with the period P for the *class-E* and *-F* stars: the class-E stars showing significantly less scatter than the *class-F* stars (Fig. 3b).

3.2.2. CO flux , gas and dust mass-loss rate

We have used the quantity $F_{CO}V_e$ (hereafter $dM_{g,co}/dt$) as a rough measure of the mass-loss rate, dM_g/dt, since the mass-loss rate should scale approximately as $T_{mb}V_e^2D^2$ (F_{CO} is the integrated CO (J=2–1) flux ($\int T_{mb}dV$) divided by the K-band flux, which, assuming that the absolute K-magnitudes of S stars are similar (Jura 1988), scales as D^{-2}, D being the stellar distance). F_{CO} refers to the CO J=2–1 flux as measured with the IRAM 30-m: for objects observed in the J=2–1 line only with the SEST 15-m or the NRAO 12-m (Bieging and Latter 1994), the measured F_{CO} has been scaled up by factors determined from a comparison of fluxes for objects common to the observations on these telescopes and the IRAM 30-m. The scaling factors are consistent with the sources being spatially unresolved sources, in which case the flux scales inversely as the square of the observing beam-sizes. A log-log plot of $dM_{g,co}/dt$ versus ΔIR_e is shown in Fig. 4a: a mass-loss rate scale based on $dM_g/dt = 1.4 \times 10^{-5}$ M$_\odot$ yr^{-1} in W Aql (Jura 1988) is shown for convenience. Determining dM_g/dt more accurately from the CO lines requires a fully self-consistent model and good J=1–0 and 2–1 data (Sahai 1990), and is not attempted here. We find that $dM_{g,co}/dt$ is strongly correlated with the infrared excess, irrespective of the circumstellar class, and that there is a remarkable change in the slope $d(\log dM_{g,co}/dt)/d(\log\Delta IR_e)$ with the LRS class , which increases from 1.3 for *class-E* to 3.1 for *class-F* and $\sim$ 8 for *class-S* stars. We also find a general increase in $dM_{g,co}/dt$ with the period (Fig. 4b).

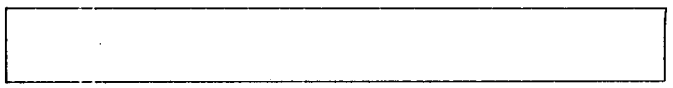

Fig. 4. The quantity F_{CO} V_e, an empirical measure of the gas-mass loss rate, plotted versus (a) infrared-excess (ΔIR_e), (b) period (P) (symbols as in Fig. 3). A mass-loss rate scale based on $dM_g/dt = 1.4 \times 10^{-5}$ M$_\odot$ yr^{-1} in W Aql (Jura 1988) is shown on the right

Dust mass-loss rates, dM_d/dt, have been calculated from the 60 μm flux, and the near-IR photometry (Gezari et al. 1993) using the formulation given by Sahai (1990). We have assumed a far-IR (60 μm) dust emissivity equal to 150 cm^2 g^{-1} and a near-IR (1 μm) absorption coefficient $Q(\lambda) = 0.24$ (both varying as λ^{-1}), a grain radius and material density, respectively equal to 0.1 μm and to 2 g cm^{-3}. Distances have been taken from Jura (1988), or calculated accordingly. The dust mass-loss rate, dM_d/dt, depends on the drift velocity of the dust through the gas, V_{dr}, and thus on the gas mass-loss rate, dM_g/dt, which is not known. Assuming that significant grain sputtering sets an upper limit of $\sim$ 20 km s^{-1} on V_{dr} (Kwok 1975), we have derived *upper limits* to the dust mass-loss rates ($dM_{d,u}/dt$) and *lower limits* to the gas mass-loss rate ($dM_{g,l}/dt$) and the gas-to-dust density ratio, $\rho_{g,l}/\rho_d$ (Table 1). A *lower limit* to the dust mass-loss rate, $dM_{d,l}/dt$, is derived by assuming $V_{dr} = 0$. Thus, for stars with large V_e (10–20 km s^{-1}) the dust mass-loss rate is restricted to a relatively small range between $dM_{d,u}/dt$ and $dM_{d,l}/dt$.

The "non-dusty" *class-S* stars have non-zero dust mass-loss rates, because although they have the lowest ΔIR_e's, these are not zero. However, this is not a contradiction of the Chen & Kwok classification, since small amounts of circumstellar dust may not be detected in the LRS spectra, which have lower sensitivity than the wide-band 25 and 60 μm fluxes, and being at shorther wavelengths, sample hotter dust closer to the star. Most stars are found to have gas-to-dust density ratios $\gtrsim$ 1000, and an effective absorption coefficient, $< Q >$, of typically 0.13. Stars with large ΔIR_e's ($\geq 10^{-0.8}$) tend to have large dust mass-loss rates (S Cas, TT Cen, S516, S Lyr, W Aql, DB42141, and WY Cas) as expected, and $< Q >$ is significantly lower (0.064–0.11). If the dust-to-gas ratios in the high-ΔIR_e stars were also > 1000 (as for the majority of stars in the sample), their gas mass-loss rates would be significantly higher than our derived lower limits, a conclusion consistent with estimates from CO data (e.g. $dM_{g,l}/dt = 9.4 \times 10^{-7}$ compared to 1.4×10^{-5} M$_\odot$ yr^{-1} in W Aql). Most of our S stars have luminosities in the range 0.7–1 $\times 10^4$ L$_\odot$, and gas mass-loss rates $\gtrsim 2 \times 10^{-7}$ M$_\odot$ yr^{-1}, a factor $\approx$ 3 larger than values derived by Jura (1988) using assumed values of the gas-to-dust ratio (220), outflow velocity (10 km s^{-1}, taken to be the same for gas and dust), and luminosity (10^4 L$_\odot$). It would be useful to derive the properties of O-rich and C-rich star CSEs as shown above, for comparison with the S stars. Olofsson et al (1993) have analysed their C star sample in a similar fashion, but have inappropriately assumed a fixed $Q = 0.015$ for all objects, based on a model of IRC+10216 whose flux peaks at significantly longer wavelengths than most stars in their sample.

4. Discussion

The mass-outflow properties of our S stars sample provide qualitative support for numerical models of mass-loss from radially pulsating red giant atmospheres, presented by Bowen (1988, hereafter B88). In these models, for a given initial mass, as evolution proceeds, the stellar luminosity and radius increase, and therefore the period increases; further as the surface gravity decreases, the scale height, the gas and dust density at a given radius, and the mass-loss rate increase. With a fixed cross-section for radiation pressure on dust, the expansion velocity also increases as the star evolves (Bowen, private communication). Differences in the initial stellar mass add complexity to the relationships between expansion velocity, amount of dust (ΔIR$_e$), mass-loss rate and period. Thus, in general, the correlations presented in Fig. 3 and 4 can be understood as a combination of stellar evolution and variations in initial stellar mass. Furthermore, in the B88 models mass-loss is obtained even without the presence of dust, due to a pressure gradient in the extended atmosphere (Bowen and Willson 1991): the non-dusty models produce dM_g/dt and V_e factors of $\approx 1/10$ and $\approx 1/5$ times smaller than corresponding values for dusty models.

Our detection of mass-outflows in stars with little or no dust (*class-S*), the weakening of the V_e–ΔIR$_e$ correlation for small ΔIR$_e$, and the sharp increase in the slope of the dependence of d$M_{g,co}$/dt on ΔIR$_e$ in going from *class-E* to *class-F* and *-S* stars, does suggest that when the amount of dust becomes very small, some mechanism other than radiation pressure on dust grains, becomes increasingly important in driving the mass-loss. However, model mass-loss rates are smaller than those deduced from our data, the discrepancy being largest for stars with small infrared excesses and short periods. For example, B88 finds, in models with no dust, with stellar mass equal to 1.2–0.8 M$_\odot$ and period of 250 days, that dM_g/dt = 3 – 20$\times 10^{-10}$ M$_\odot$ yr^{-1} (dM_g/dt is smaller for shorter periods, and larger stellar masses), whereas we find dM_g/dt $> 2 \times 10^{-7}$ M$_\odot$ yr^{-1} for the two *class-S*, short period stars AA Cyg (P = 213 days) and RX Lac (P = 174 days). In the dusty models, with M =2–0.8 M$_\odot$ and P = 250 days, dM_g/dt=0.9–30 $\times 10^{-8}$ M$_\odot$ yr^{-1}, as compared with dM_g/dt > 2.3–7.5 $\times 10^{-7}$ M$_\odot$ yr^{-1} for eight *class-F* and *-E*, short-period (110–223 days) stars in our sample. Better agreement with the data may be achieved in the B88 models by adopting higher values of the luminosity L (note that our estimates of L for the observed stars are, in fact, generally higher than the model value, 5.3×10^3 L$_\odot$) and lower values of $T_{\rm eff}$ (assumed to be 3000K by B88 but largely undetermined). Theoretical efforts to explain the *changes* in the V_e – ΔIR$_e$ and d$M_{g,co}$/dt – ΔIR$_e$ relationships as a function of LRS class found in our study are urgently needed, and should provide new insights into the nature of mass-loss in AGB stars.

Acknowledgements. R. Sahai acknowledges support from the Swedish Naturvetenskapliga Forskningsrådet (grant 9098-312), the Jet Propulsion Laboratory, California Institute of Technology (under contract to the National Aeronautics and Space Administration), and the National Research Council (National Academy of Sciences). S. Liechti thanks the Max-Planck Institut für Radioastronomie and the Spanish CICYT (grant number PB90-408) for their partial economic support during this work.

References

Bieging, J.H., Latter, W.B. 1994, ApJ, 422, 765
Bowen, G.H. 1988, ApJ, 329, 299
Bowen, G.H., Willson, L.A. 1991, ApJ, 375, L53
Chen, P.S., Kwok, S. 1993, ApJ, 416, 769
Groenewegen, M.A.T., A&A, 1993, 271, 180
Jorissen, A. et al. 1993, A&A, 271, 463
Jura, M. 1988, ApJS, 66, 33
Kahane, C., Maizels, C., Jura, M. 1988, ApJ, 327, L23
Knapp, G.R. 1986, ApJ, 311, 731
Kwok, S. 1975, ApJ, 198, 583
Loup, C., Forveille, T., Omont, A., Paul, J.F. 1993, A&AS 99, 291
Margulis, M., Van Blerkom, D.J., Snell, R.L., Kleinmann, S.G. 1990, ApJ, 361, 673
Neugebauer, G., Leighton, R.B. 1969, Two-Micron Sky Survey-A Preliminary Catalog, NASA SP-3047
Olofsson, H., Eriksson, K., Gustafsson, B., Carlström, U. 1994, ApJS, 87, 267
Olofsson, H., Carlström, U., Eriksson, K., Gustafsson, B., Willson, L.A. 1990, A&A, 230, L13
Plaut, L. 1977, A&AS, 28, 169
Sahai, R., Wannier, P.G. 1988, A&A, 201, L9
Sahai, R. 1992, A&A, 253, L33
Sahai, R. 1990, ApJ, 362, 652
Scalo, J.M., Ross, J.E. 1976, A&A, 48, 219
Stephenson, C.B. 1984, A General Catalogue of Galactic S stars, 2nd Ed., Publications of the Warner and Swasey Observatory, Vol. 3, No. 1
Wannier, P.G., Sahai, R., Andersson, B-G., Johnson, H.R. 1990, ApJ, 358, 251
Wannier, P.G., Sahai, R. 1986, ApJ, 311, 335
Wing, R.F., Yorka, S.B. 1977, MNRAS, 178, 383

This article was processed by the author using Springer-Verlag LaTeX A&A style file 1990.

Table 1. Survey S Stars

Source	α(1950)	δ(1950)	CO J_{up}/θ_b(")	T_p (mK)	rms (mK)	Filt. (MHz)	V_e (km s^{-1})	V_c (km s^{-1})	α	L ($10^4 L_o$)	<Q>	$M_{g,l}$ (10^{-7} ($M_o yr^{-1}$)	$M_{d,u}$ (10^{-9})	$M_{d,l}$ (10^{-9})	log (ρ_g/ρ_d),l	Class[a]
V365 Cas	005753.5	562035	2/13	65±10	17	2	7.2±0.8	-2.1±0.7	1.0	1.9	0.12	8.8	0.37	0.10	3.95	S, F
BD Cam[b]	033747.1	630323	2/13	...	47	1	...	...	...	...	...	...	...	...	...	S, S
T Cam	043512.2	660253	2/13	...	43	1	...	...	...	...	...	....	....	...	...	S, S
o^1 Ori	044942.0	141004	1/45	...	18	0.7	...	...	...	...	...	...	...	...	...	MS, S
S 98[g]	051953.0	-084305	1/45	...	11	0.7	...	...	...	...	...	...	...	...	...	S, S
NO Aur	053726.4	315343	2/13	...	46	1	...	...	...	...	...	...	...	...	...	MS, E
FU Mon	061945.8	032701	1/45	75[c]±	12	0.7	29±1.6	-15±0.2	-1	1.8	0.13	33	1.7	1.0	3.52	S, S
DY Gem	063307.7	141517	2/13	250±20	49	1	8.0±0.13	-16.0±0.1	0.1	0.69	0.13	3.7	1.3	0.37	3.01	S, F
R Gem	070420.5	224657	2/13	1400±20	120	0.1	4.8±0.07	-59.1±0.05	1	0.70	0.14	2.4	1.5	0.29	2.92	S, F
AA Cam	070933.6	685325	2/13	59±7	23	2	17.9±0.8	-43.5±0.7	0.3	0.81	0.13	9.5	1.1	0.52	3.25	MS, F
RR Mon	071456.5	011109	1/45	...	9	0.7	...	...	...	...	...	...	...	...	...	MS, E
			2/13	...	21	2	...	...	...							
SU Mon	073955.9	-104541	1/45	...	12	0.7	...	...	...	...	...	...	...	...	...	S, S
S 327	084021.9	-385323	1/45	i.s.[d]	16	0.7	...	...	...	...	...	...	...	...	...	S, F
UU Vel	093353.7	-534954	1/45	i.s.	110	0.7	...	...	...	...	...	...	...	...	...	S, E
UY Cen	131336.6	-442625	2/23	57±4	16	0.7	13.1±0.2	-28.6±1.3	-0.5	0.93	0.12	7.5	0.72	0.28	3.42	S, C
TT Cen	131621.6	-603100	1/45	54±12	38	0.35	24±2.5	5.2±1.5	0.8	0.63	0.11	8.7	15	8.2	2.01	SC, F
			2/23	240±4	50	0.17	25.4±0.1	5.5±0.3	1							
S 468	133714.8	-713653	1/45	i.s.	10	0.7	...	...	...	...	...	...	...	...	...	S, S
AM Cen	134404.6	-530630	1/45	80	22	0.35	...	...	...							
							5.4[e]±0.3	-27.4[e]±0.3	1[e]	0.72	0.13	2.6	1.1	0.23	3.06	SC, S
			2/23	200	37	0.17	...	...	...							
VX Cen	134745.9	-600947	1/45	...	38	0.17	...	...	...	...	...	...	...	...	...	S, S
GI Lup	150300.4	-411641	1/45	...	46	0.17	...	...	...	0.98	0.11	7.7	1.3	0.54	3.16	S, F
			2/23	100±5	41	0.17	14±1	6±1.5	1							
ST Her	154916.0	483755	2/13	450±10	95	0.1	9.1±0.12	-4.4±0.1	0.5	0.70	0.14	4.4	0.85	0.27	3.22	MS, E
S 504	162407.2	-561425	1/45	...	7.8	0.7	...	...	...	...	...	...	...	...	...	S, ?
ST Sco	163324.8	-310759	1/45	140±10	23	0.7	7.3±0.5	-1.2±0.4	1	0.75	0.13	3.5	0.72	0.19	3.26	S, E
RT Sco	170009.2	-365100	1/45	200±7	20	0.7	13.1±0.4	-44.5±0.3	0.8	0.98	0.11	6.1	3.1	1.1	2.74	S, E
			2/23	180±7	54	0.7	9.6±0.03	-44.4±0.04	0							
TV Dra	170806.2	642253	2/13	300±10	87	0.1	5.1±0.13	21.2±0.1	0.8	0.82	0.13	2.8	0.64	0.13	3.33	S, ?
S 516	171026.5	-314649	1/45	28±3	8.8	0.7	18.2±0.8	25.5±0.6	0.2	1.1	0.10	11	38	19	1.76	S, ?
			2/23	81±7	20	0.7	21.9±1.6	23.5±1.0	1							
V521 Oph	172040.0	-282604	1/45	i.s.	10.9	0.7	...	...	...	...	...	...	...	...	...	S, ?
S 533	174851.4	-280040	1/45	i.s.		0.7	...	...	...	...	...	...	...	...	...	S, ?
V407 Sco	174905.5	-350238	1/45	...	9.0	0.7	...	...	...	...	...	...	...	...	...	S, ?
VX Aql	185733.3	-013914	1/45	...	120	0.7	...	...	...							
			2/23	50±5	11	0.7	7.8±0.4	6.7±0.4	0.3	0.77	0.11	3.4	2.7	0.75	2.66	SC, ?
ST Sgr	185840.4	-124953	1/45	61±3	6.6	0.7	9.6±0.4	55.1±0.3	1	0.55	0.12	3.3	1.5	0.51	2.81	S, E
			2/23	110±10	31	0.7	11.2±0.6	49.8±0.5	1							
S Lyr	191108.3	255516	2/13	400±8	40	0.1	13.9±0.1	51.2±0.1	0.7	1.9	0.077	9.9	25	10	1.98	SC, E

Table 1 (*continued*). **Survey S Stars**

Source	α(1950)	δ(1950)	CO J_{up}/θ_b(")	T_p (mK)	rms (mK)	Filt. (MHz)	V_e (km s^{-1})	V_c (km s^{-1})	α	L ($10^4 L_\odot$)	<Q>	$M_{g,l}$ (10^{-7} ($M_\odot yr^{-1}$)	$M_{d,u}$ (10^{-9})	$M_{d,l}$ (10^{-9})	log $(\rho_g/\rho_d)_{,l}$	Class[a]
W Aql	191242.0	-070807	1/45	1300±35	230	0.17	18.3±0.2	-24.1±0.2	0.8	1.6	0.064	9.4	35	17	1.75	S, E
			2/23	2040±40	250	0.7	18.0±0.2	-24.3±0.2	0.9							
			2/13	6050±40	160	1	18.8±0.08	-24.0±0.06	0.7							
T Sgr	191321.0	-170340	1/45	...	16	0.7	...	...	...							
			2/23	59±4	22	0.7	14.1±0.5	10.8±0.4	0.2	0.95	0.12	8.1	1.8	0.74	3.05	S, F
EP Vul	193110.3	233243	1/45	76±7	12	0.7	5.6±0.5	-0.7±0.3	1	0.69	0.14	2.2	0.64	0.13	3.25	S, F
			2/13	520±20	135	0.1	4.7±0.1	-0.05±0.10	0.7							
χ Cyg	194838.3	324708	2/13	6200±24	240	0.1	8.8±0.01	10±0.02	0.4	0.69	0.12	3.7	1.6	0.49	2.88	S, E
AA Cyg	200236.6	364024	2/13	950±20	130	0.1	4.8±0.07	27.9±0.05	0.7	0.69	0.14	2.3	0.85	0.16	3.15	S, S
DK Vul	200425.9	241717	2/13	1100±20	45	0.1	4.7±0.09	-14.2±0.07	1	0.83	0.13	2.5	1.6	0.30	2.91	S, F
S 636	201005.1	-622549	1/45	...	35	0.17	...	...	...	...	...	...	...	...	...	S, S
			2/23	...	144	0.17	...	...	...							
RZ Sgr	201200.3	-443348	1/45	360±10	27	0.7	14±0.2	-31.6±0.05	0.6	0.92	0.12	6.4	3.9	1.4	2.66	S, F
			2/23	980±10	37	0.7	8.8±0.1	-31.2±0.1	1							
CY Cyg	204508.5	455204	2/13	...	45	1	...	...	...	...	...	...	...	...	...	SC, ?
RZ Peg	220340.4	331543	2/13	210±10	37	1	12.6±0.6	-23.4±0.5	1	1.1	0.12	7.9	2.2	0.85	2.96	SC, C
π^1 Gru	221940.8	-461206	1/45	600	84	0.087										
							11[f]	-12.5[f]	...	0.76	0.13	5.3	1.3	0.46	3.05	S, E
			2/23	2000	59	0.17										
RX Lac	224740.4	404705	1/45	...	132	0.17	...	...	...							
			2/13	680±20	120	0.1	3.4±0.09	-15.4±0.07	1	0.87	0.13	1.9	0.50	0.07	3.41	S, S
DB 42141	225113.8	610058	2/13	140±8	36	1	19.6±0.84	-51.8±0.7	0.8	0.45	0.088	3.8	25	12	1.50	S, E
57 Peg	230701.7	082432	1/45	...	13	0.7	...	...	...	...	...	...	...	...	...	MS, S
			2/13	...	36	1										
WY Cas	235529.2	561233	2/13	500±10	41	1	13.3±0.2	7.5±0.2	0.6	1.0	0.095	6.4	12	4.8	2.14	S, E
W Cet	235933.3	-145724	1/45	...	36	0.7	...	...	...	...	...	...	...	...	...	S, F
R And[g]							11			1.5	0.12	9.4	3.0	1.1	2.94	S, E
S Cas							18			0.80	0.065	4.7	24.5	11.6	1.60	S, E
W And							11			1.4	0.12	9.4	2.8	0.99	2.98	S, E
Y Lyn							5.4			0.71	0.14	2.6	0.69	0.15	3.25	MS, E
R Lyn							7.7			0.49	0.13	2.4	0.91	0.25	2.97	S, F
RS Cnc							6.6			0.79	0.14	3.6	0.64	0.16	3.36	MS, E
R Cyg							10.4			1.6	0.13	11	5.7	1.9	2.75	S, E

a) spectral type & LRS class primarily from Chen and Kwok (1993), otherwise from Stephenson (1984) or Wing and Yorka (1977)
b) the coordinates used for this source, taken from the IRC catalog (Neugebauer and Leighton 1969), differ from the IRAS coordinates by 27"
c) line is fitted with a horned shape, Tmb is peak temperature in the wings
d) contamination due to interstellar emission
e) derived from a composite line-profile generated by averaging the CO 1-0 and 2-1 spectra
f) from Sahai (1992)
g) sources with names in italics were not observed in the present survey: expansion velocities for these sources are taken from Margulis et al. (1990), Knapp (1986), Wannier & Sahai (1986), and Bieging & Latter (1994) (weighted averages were computed when appropriate)

Fig 1

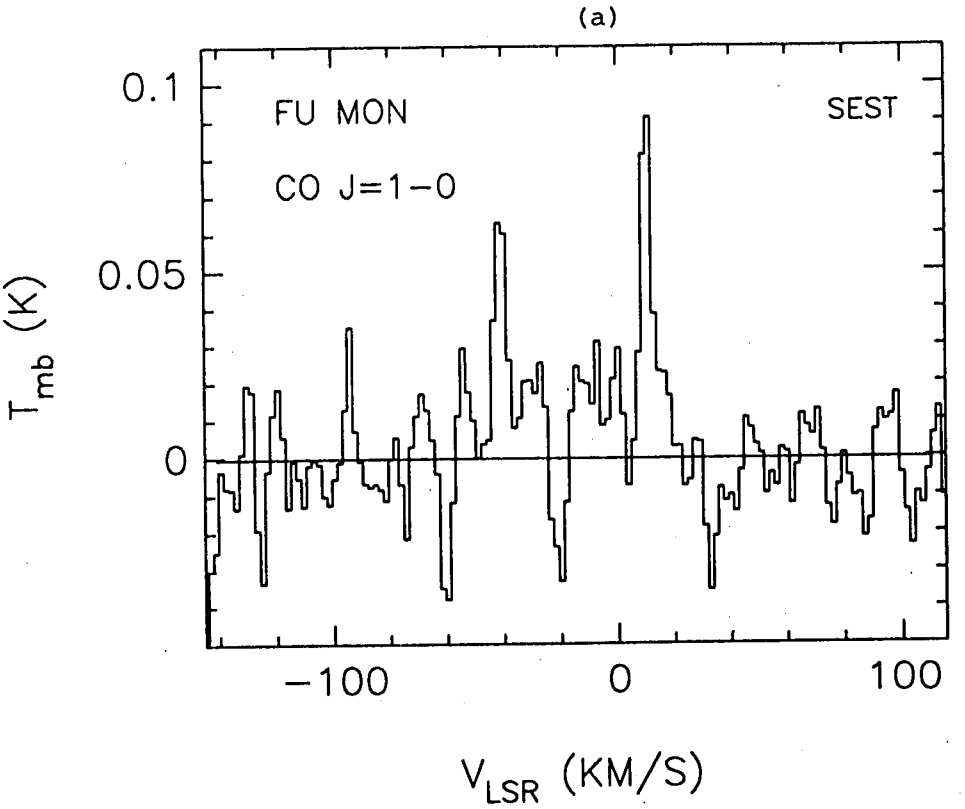
(a)
FU MON
CO J=1–0
SEST
0.1
0.05
0
T_{mb} (K)
–100
0
100
V_{LSR} (KM/S)

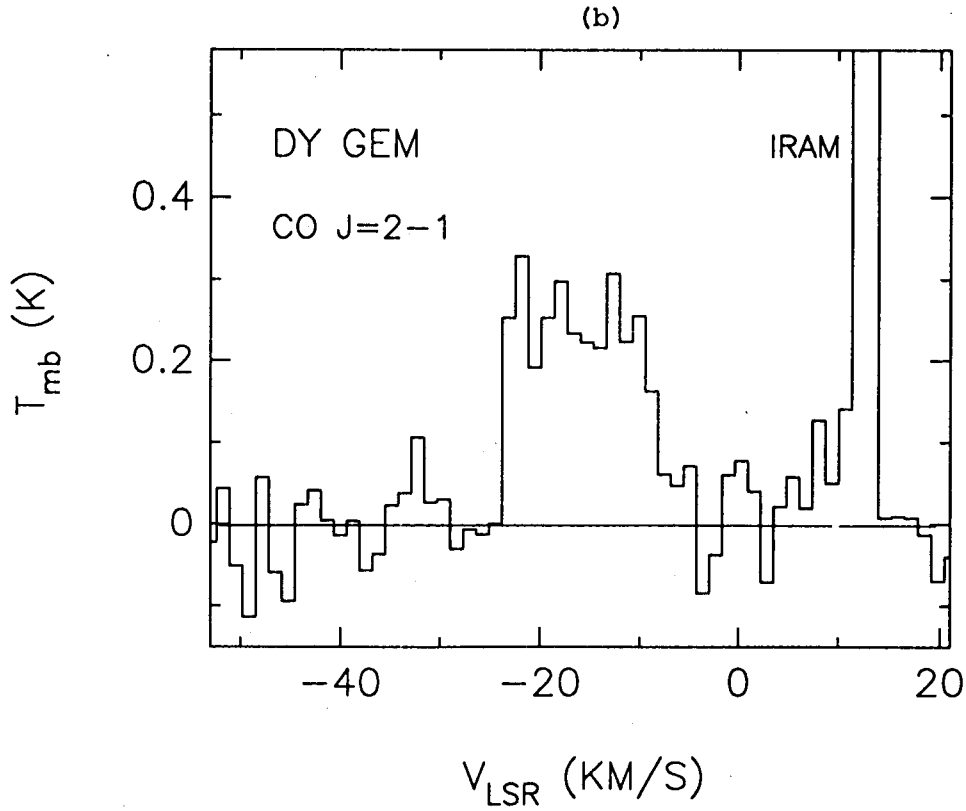
(b)
DY GEM
CO J=2–1
IRAM
0.4
0.2
0
T_{mb} (K)
–40
–20
0
20
V_{LSR} (KM/S)

Fig 1

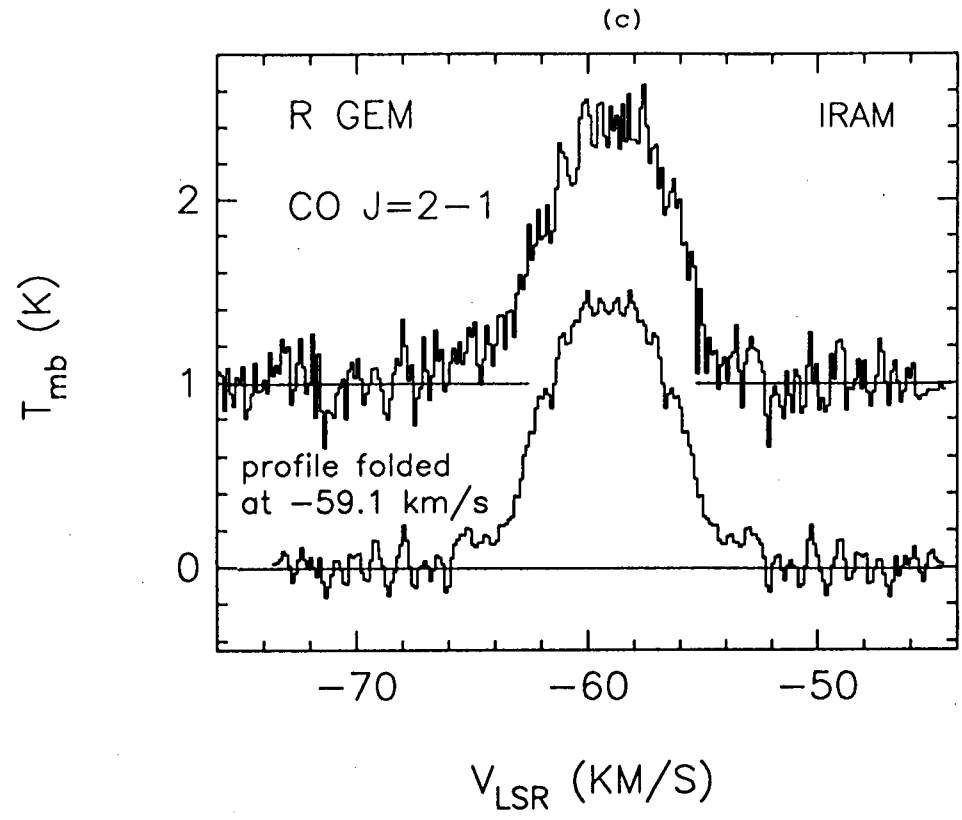
(c)
R GEM
IRAM
CO J=2−1
profile folded
at −59.1 km/s
T_{mb} (K)
2
1
0
−70
−60
−50
V_{LSR} (KM/S)

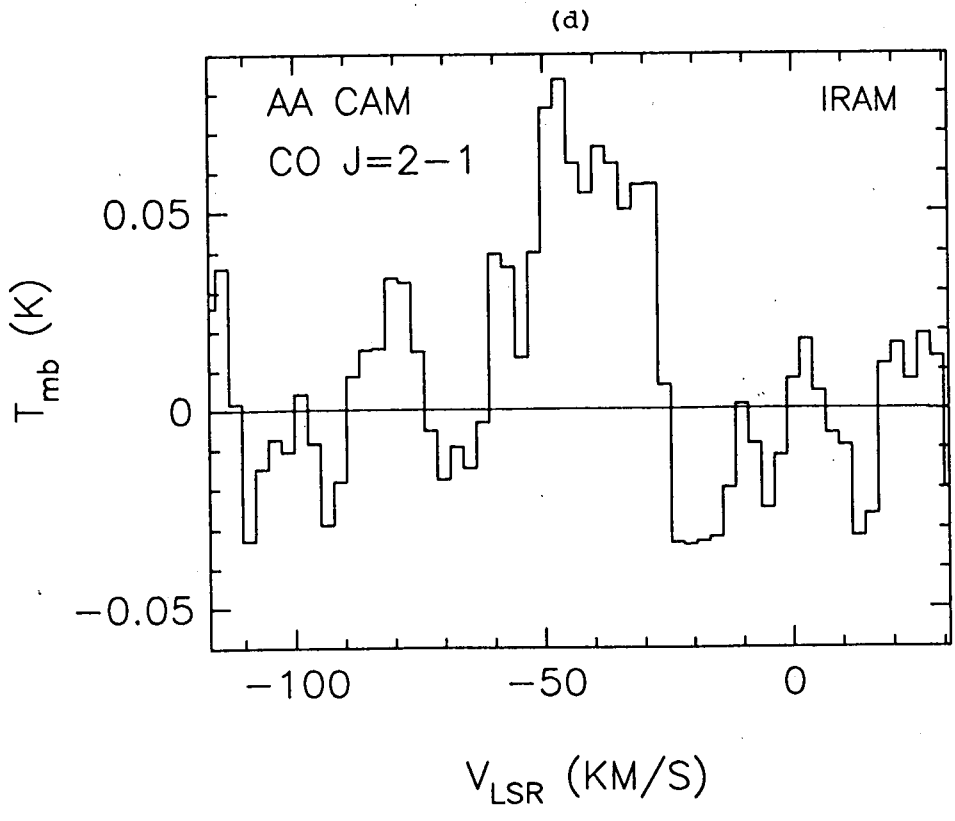
(d)
AA CAM
IRAM
CO J=2−1
T_{mb} (K)
0.05
0
−0.05
−100
−50
0
V_{LSR} (KM/S)

Fig 1

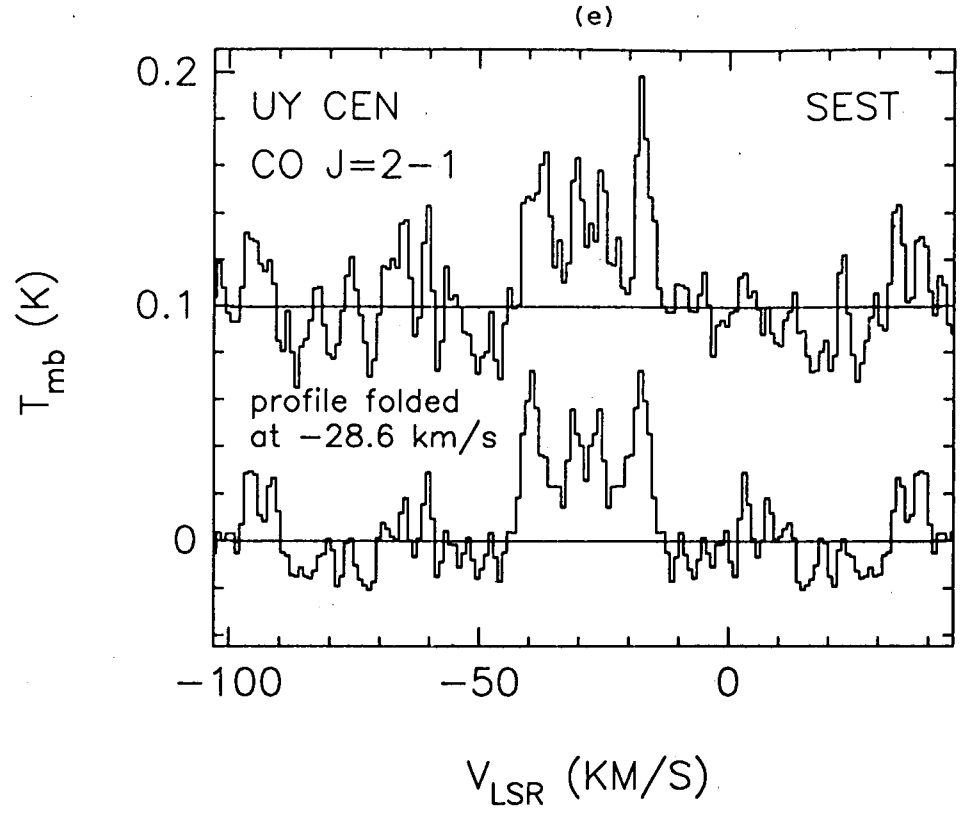
(e)
UY CEN
CO J=2−1
SEST
profile folded
at −28.6 km/s
0.2
0.1
0
−100
−50
0
T_{mb} (K)
V_{LSR} (KM/S)

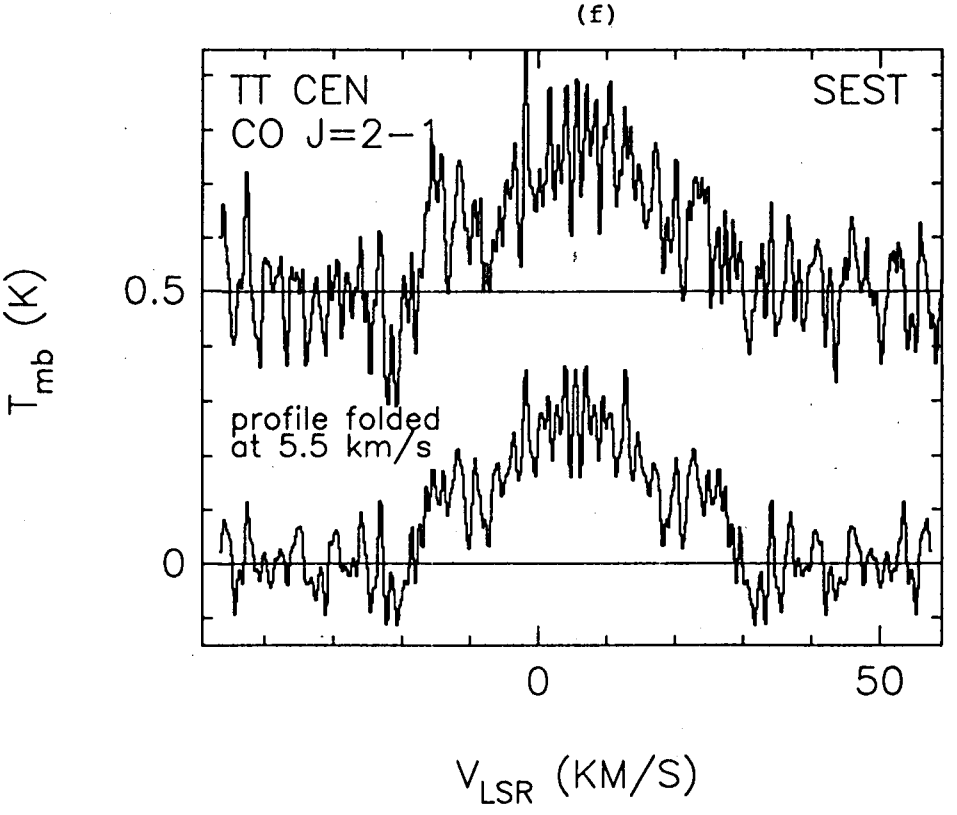
(f)
TT CEN
CO J=2−1
SEST
profile folded
at 5.5 km/s
0.5
0
0
50
T_{mb} (K)
V_{LSR} (KM/S)

Fig 1

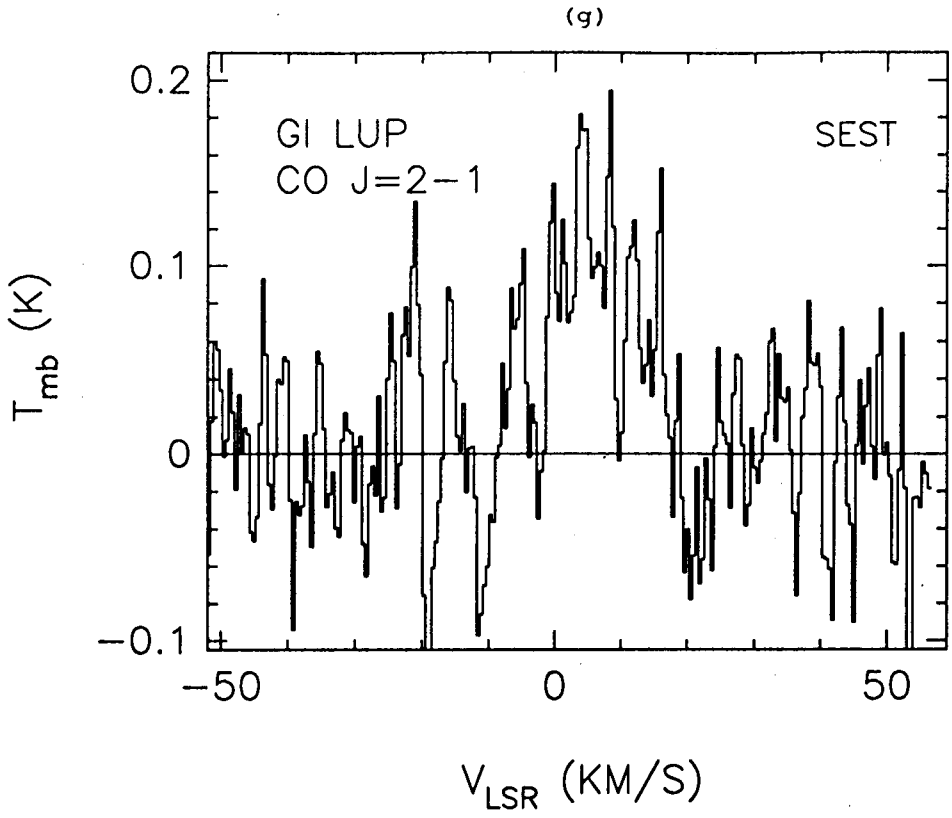
(g)
GI LUP
CO J=2−1
SEST
0.2
0.1
0
−0.1
T_{mb} (K)
−50
0
50
V_{LSR} (KM/S)

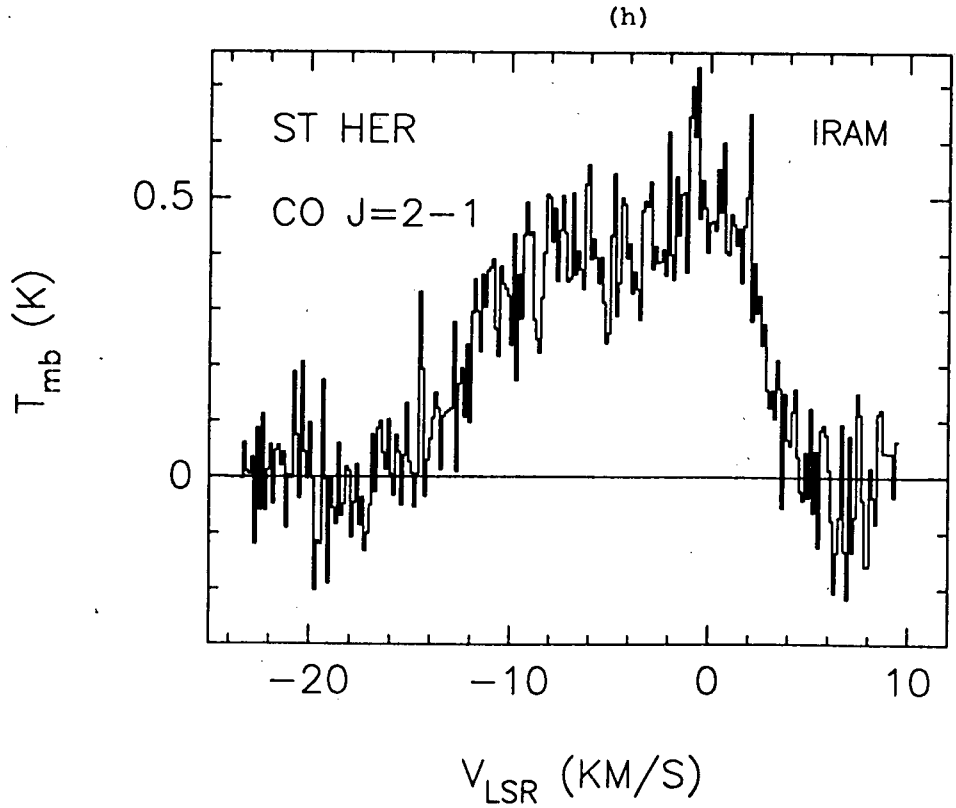
(h)
ST HER
CO J=2−1
IRAM
0.5
0
T_{mb} (K)
−20
−10
0
10
V_{LSR} (KM/S)

Fig 1.

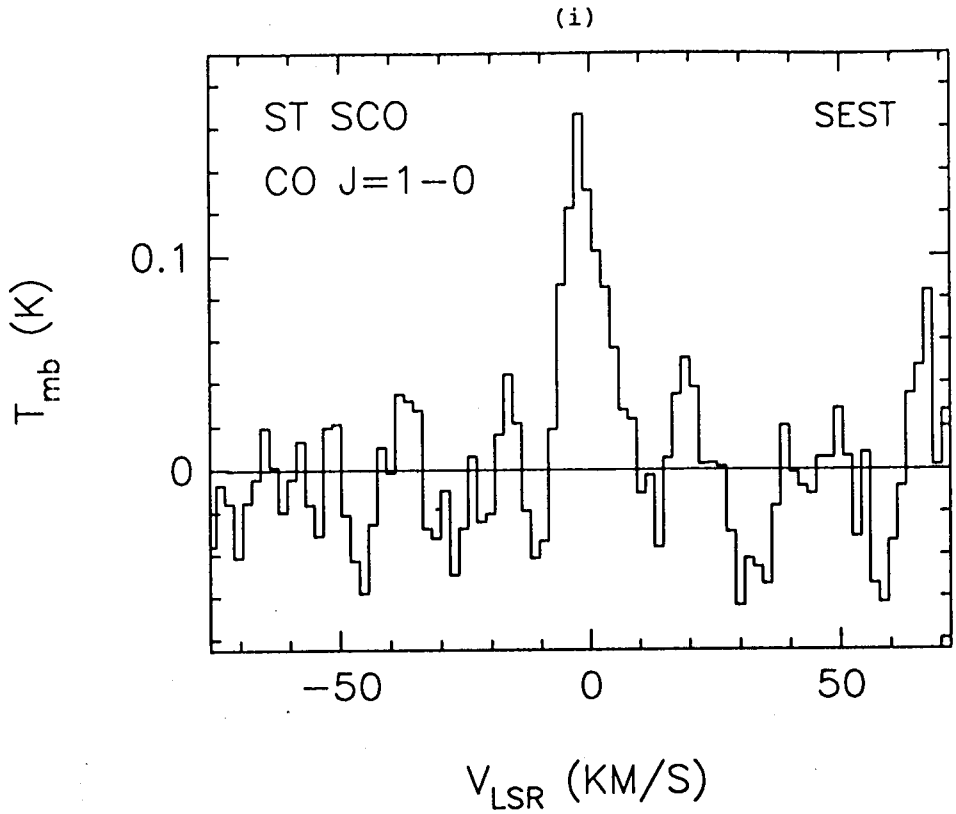
(i)
ST SCO
CO J=1−0
SEST
0.1
0
T_{mb} (K)
−50
0
50
V_{LSR} (KM/S)

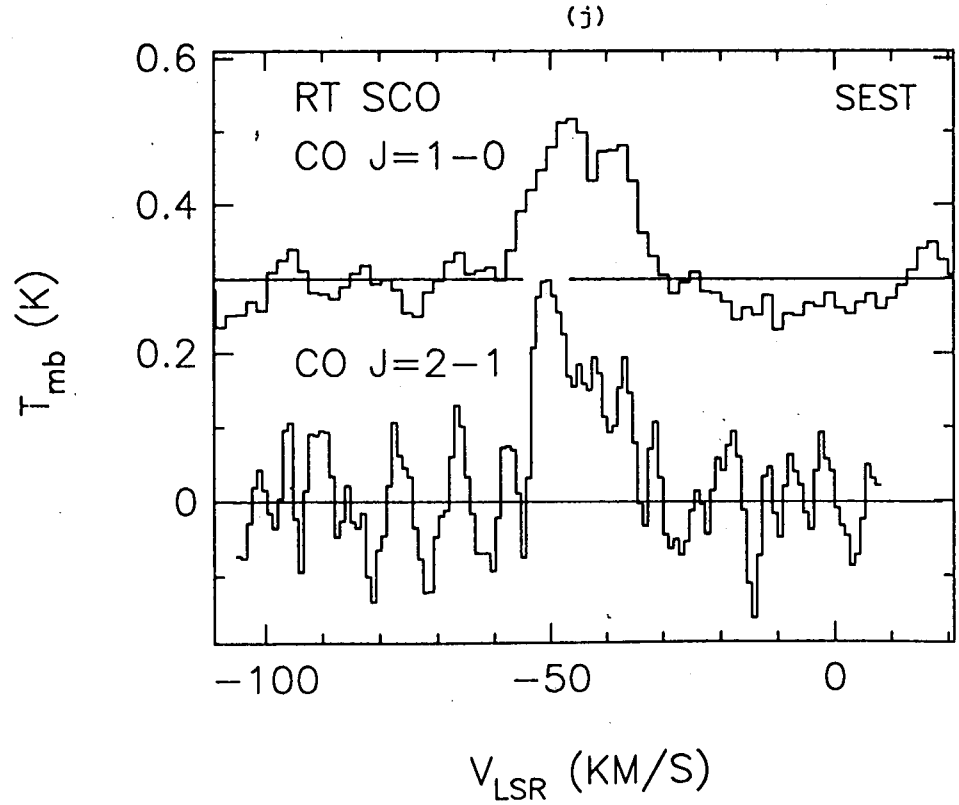
(j)
RT SCO
CO J=1−0
SEST
CO J=2−1
0.6
0.4
0.2
0
T_{mb} (K)
−100
−50
0
V_{LSR} (KM/S)

Fig. 1.

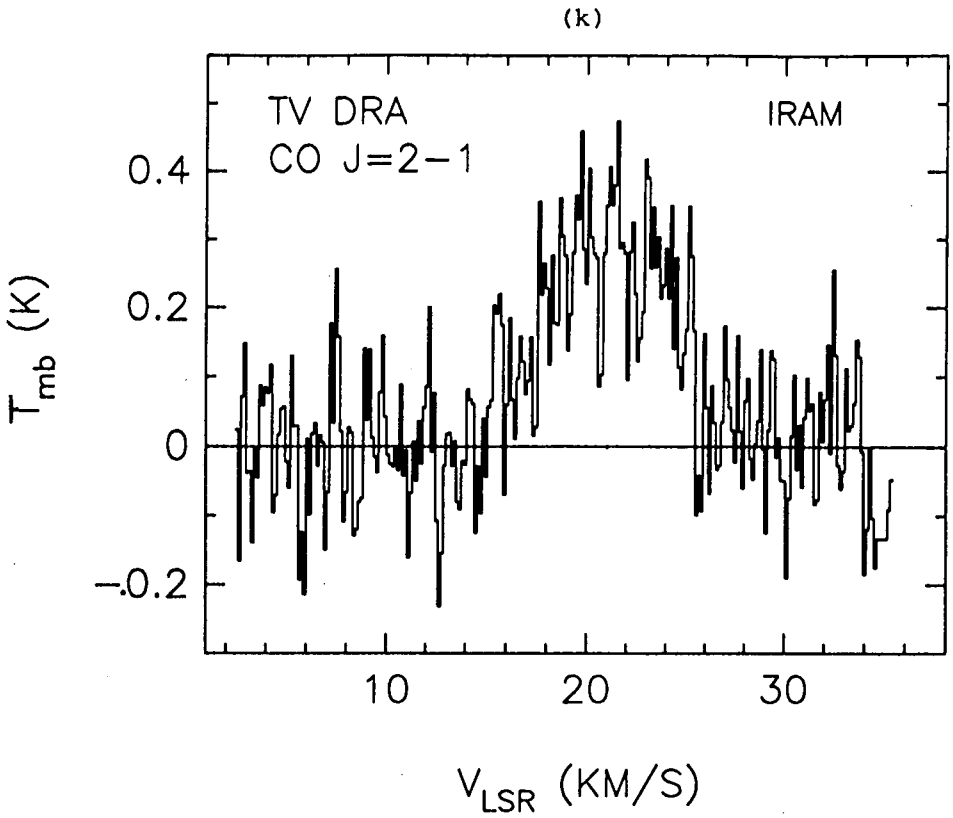
(k)
TV DRA
CO J=2−1
IRAM
0.4
0.2
0
−0.2
T_{mb} (K)
10
20
30
V_{LSR} (KM/S)

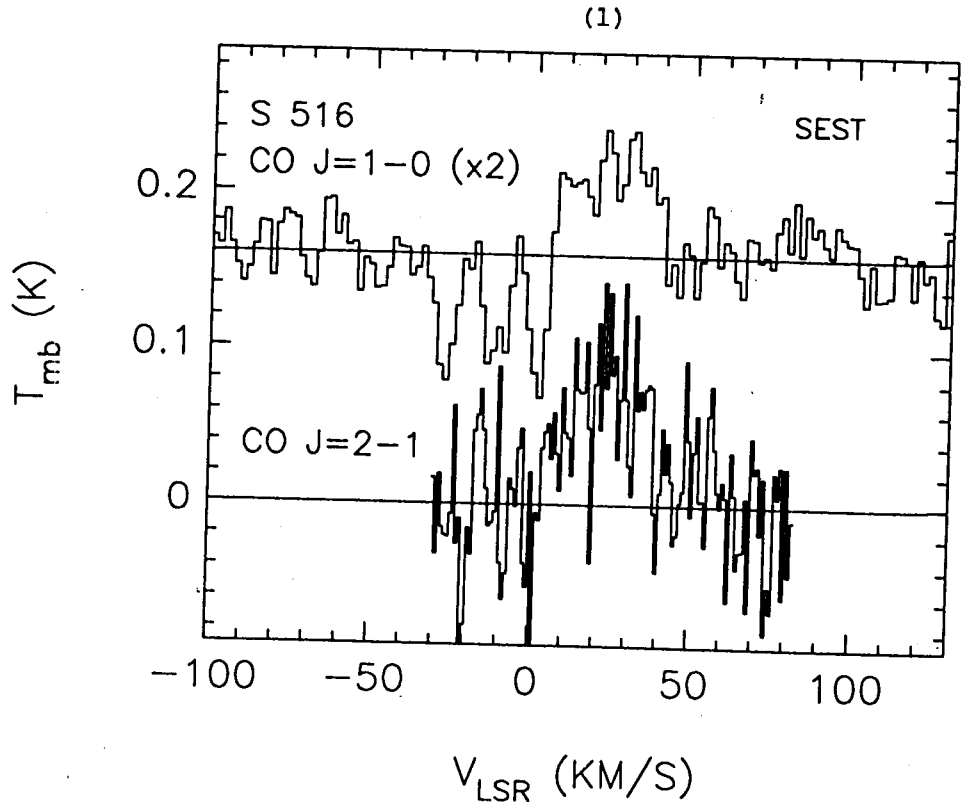
(l)
S 516
CO J=1−0 (x2)
SEST
CO J=2−1
0.2
0.1
0
T_{mb} (K)
−100
−50
0
50
100
V_{LSR} (KM/S)

Fig. 1

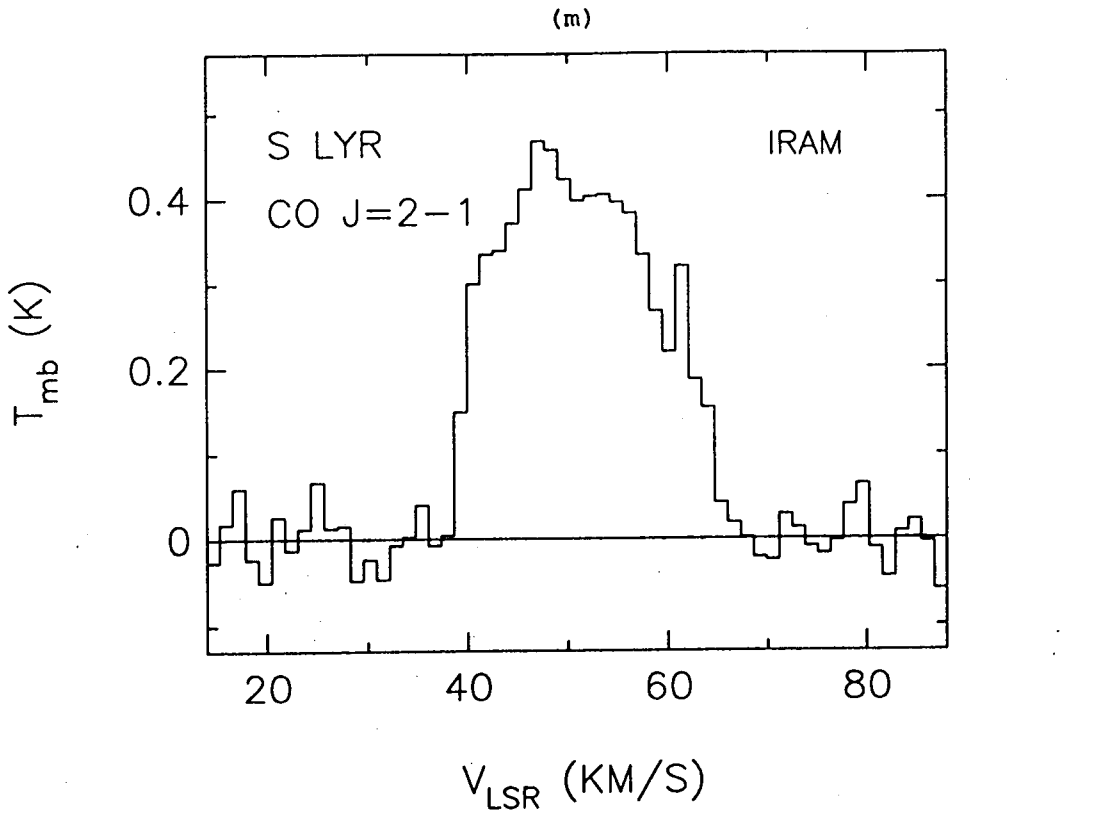
(m)
S LYR
IRAM
CO J=2−1
0.4
0.2
0
T_{mb} (K)
20
40
60
80
V_{LSR} (KM/S)

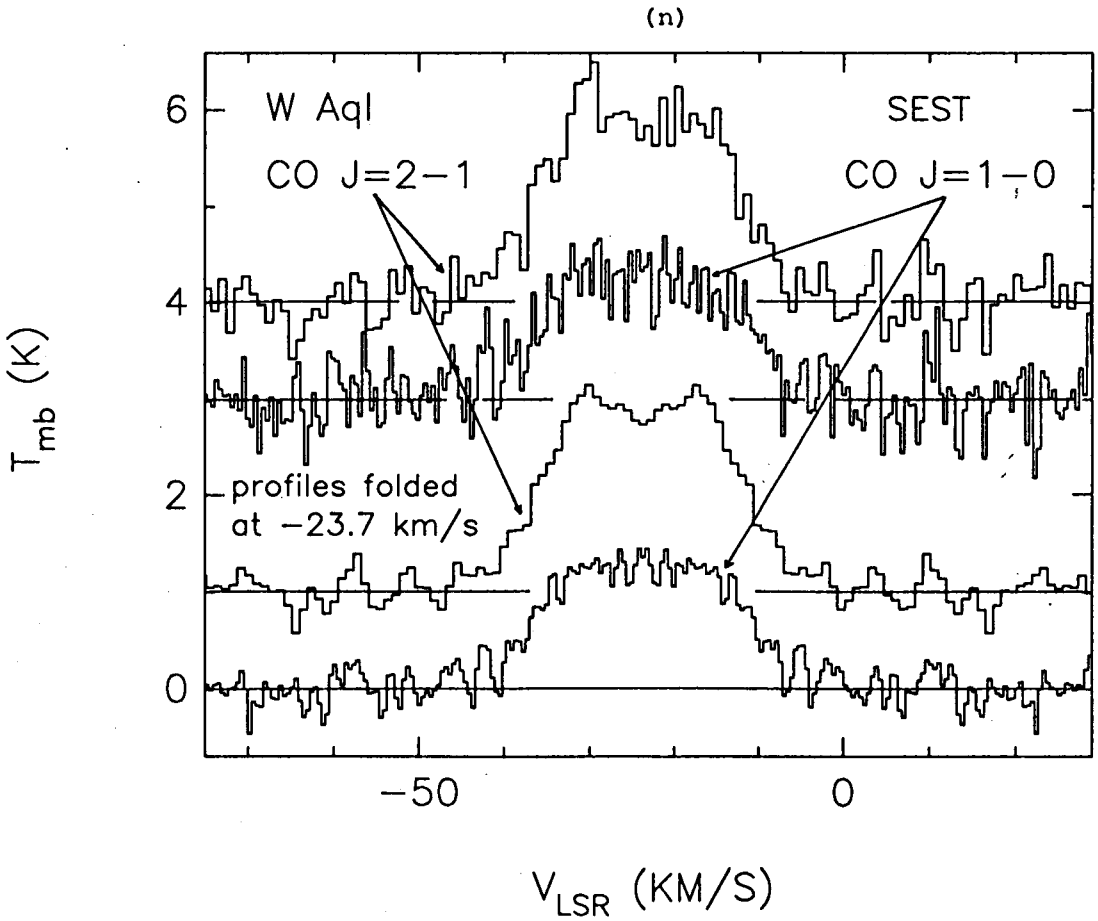
(n)
W Aql
SEST
CO J=2−1
CO J=1−0
profiles folded
at −23.7 km/s
6
4
2
0
T_{mb} (K)
−50
0
V_{LSR} (KM/S)

Fig. 1.

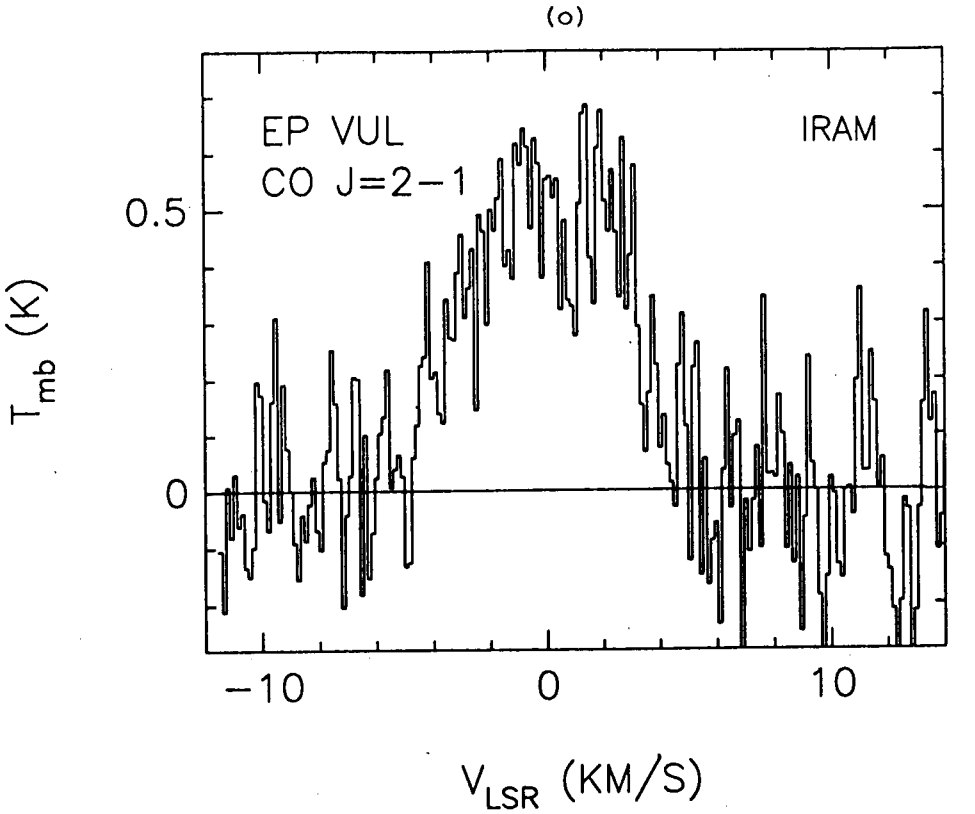
(o)
EP VUL
CO J=2−1
IRAM
0.5
0
T_{mb} (K)
−10
0
10
V_{LSR} (KM/S)

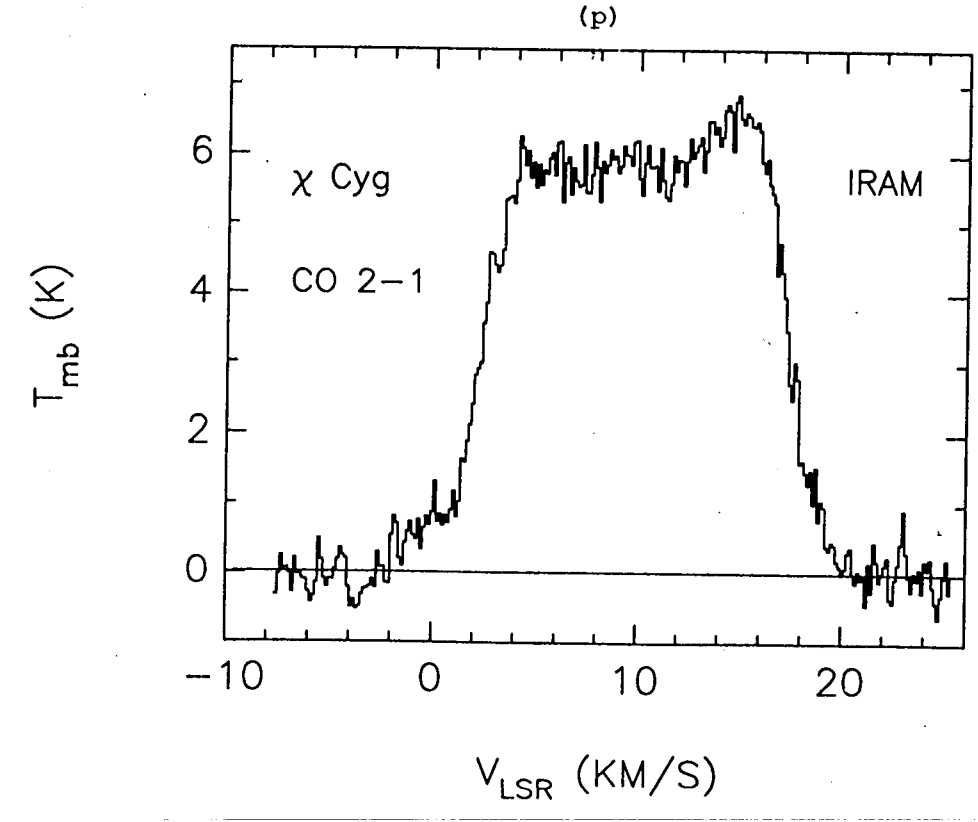
(p)
χ Cyg
CO 2−1
IRAM
6
4
2
0
T_{mb} (K)
−10
0
10
20
V_{LSR} (KM/S)

Fig. 1.

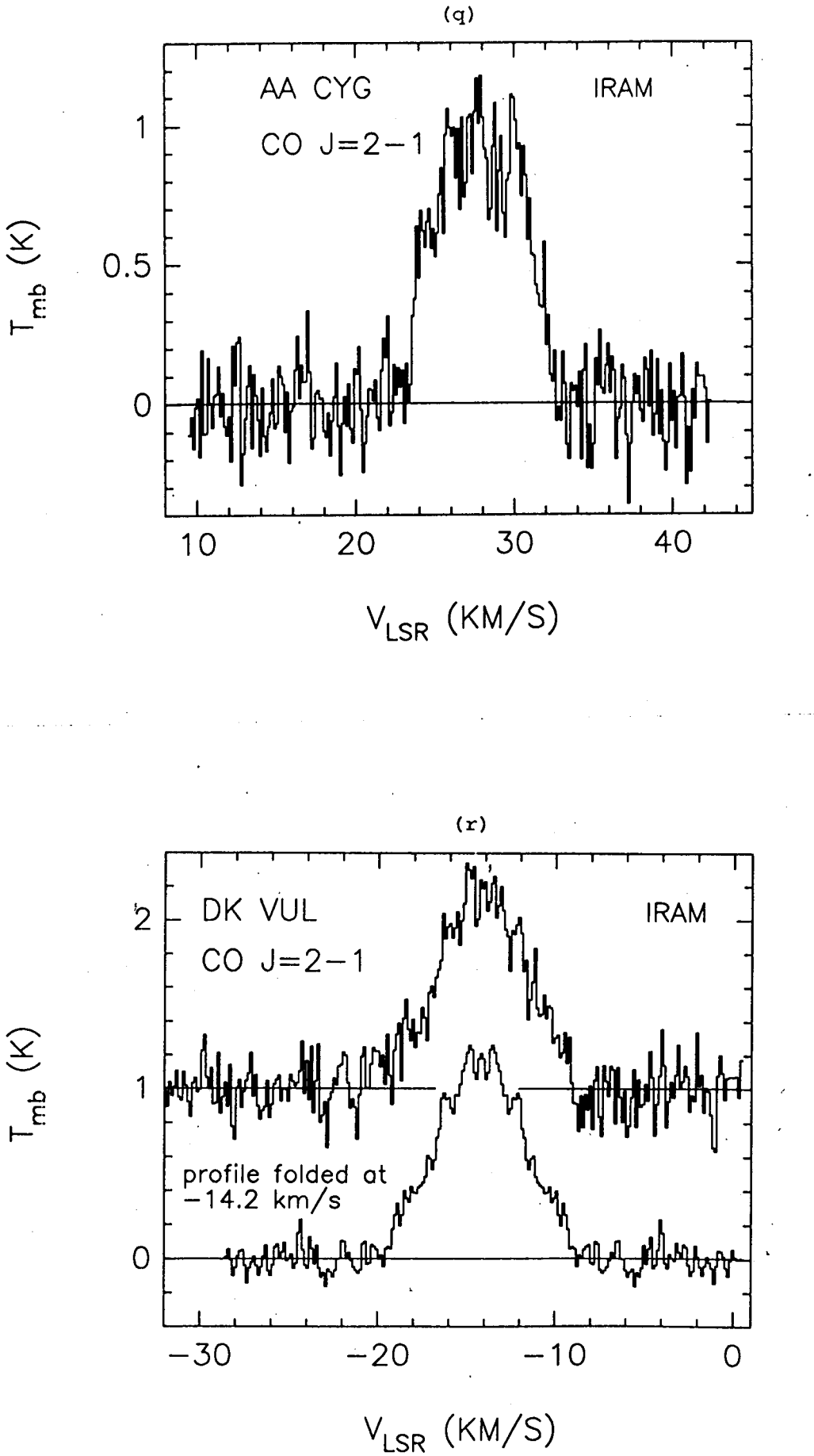
(q)
AA CYG
IRAM
CO J=2−1
1
0.5
0
T_{mb} (K)
10
20
30
40
V_{LSR} (KM/S)
(r)
DK VUL
IRAM
CO J=2−1
2
1
0
profile folded at
−14.2 km/s
T_{mb} (K)
−30
−20
−10
0
V_{LSR} (KM/S)

Fig. 1.

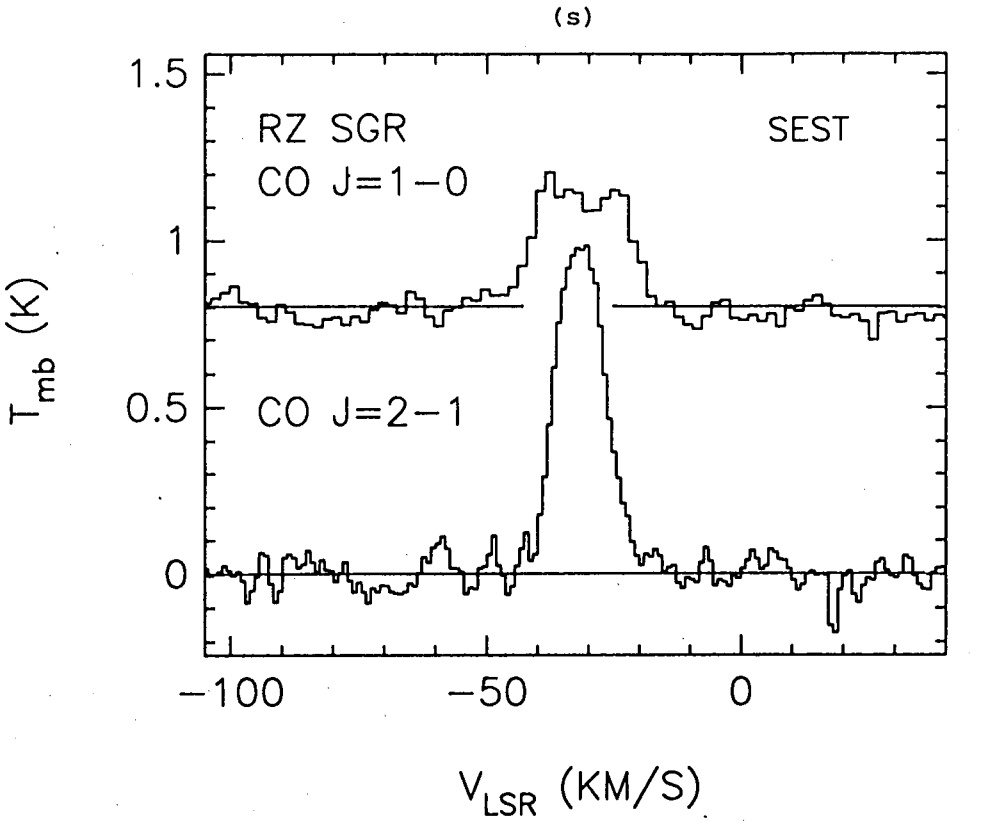
(s)
RZ SGR
SEST
CO J=1−0
CO J=2−1
1.5
1
0.5
0
T_{mb} (K)
−100
−50
0
V_{LSR} (KM/S)

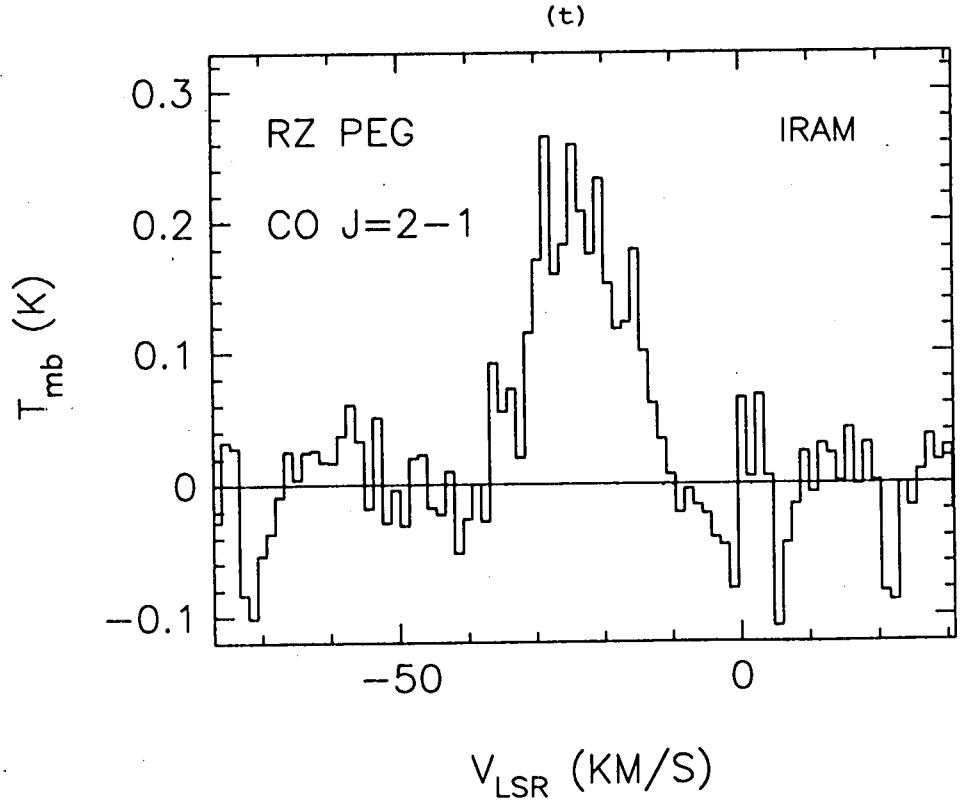
(t)
RZ PEG
IRAM
CO J=2−1
0.3
0.2
0.1
0
−0.1
T_{mb} (K)
−50
0
V_{LSR} (KM/S)

Fig. 1.

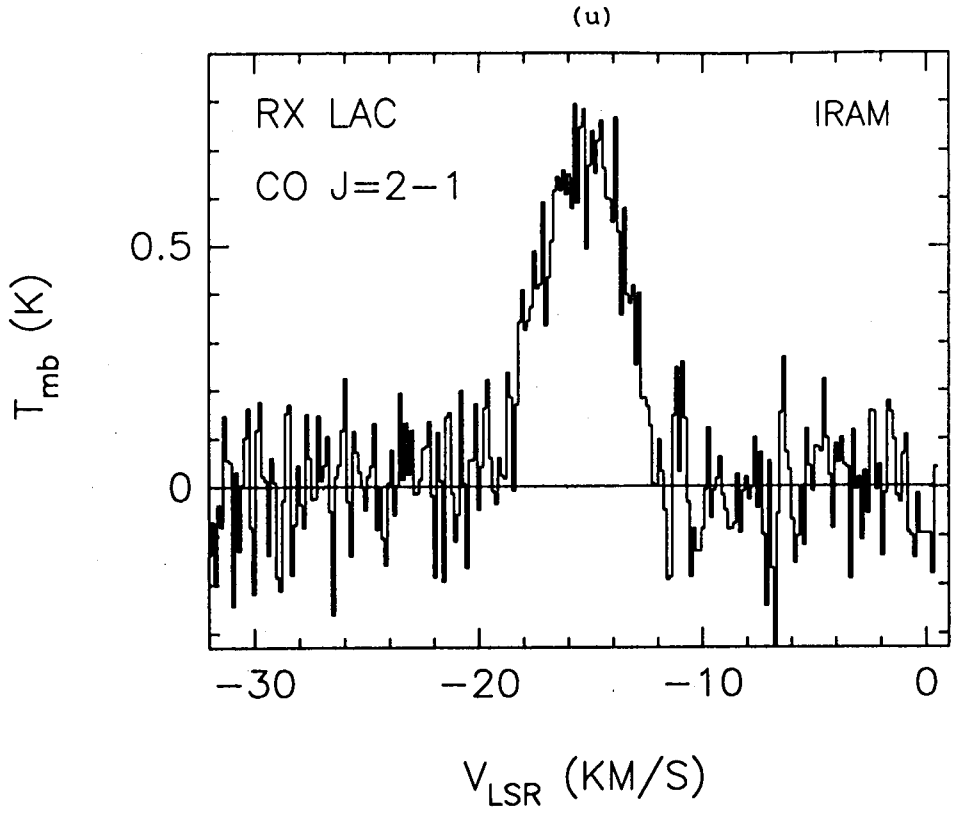
(u)
RX LAC
CO J=2−1
IRAM
0.5
0
T_{mb} (K)
−30
−20
−10
0
V_{LSR} (KM/S)

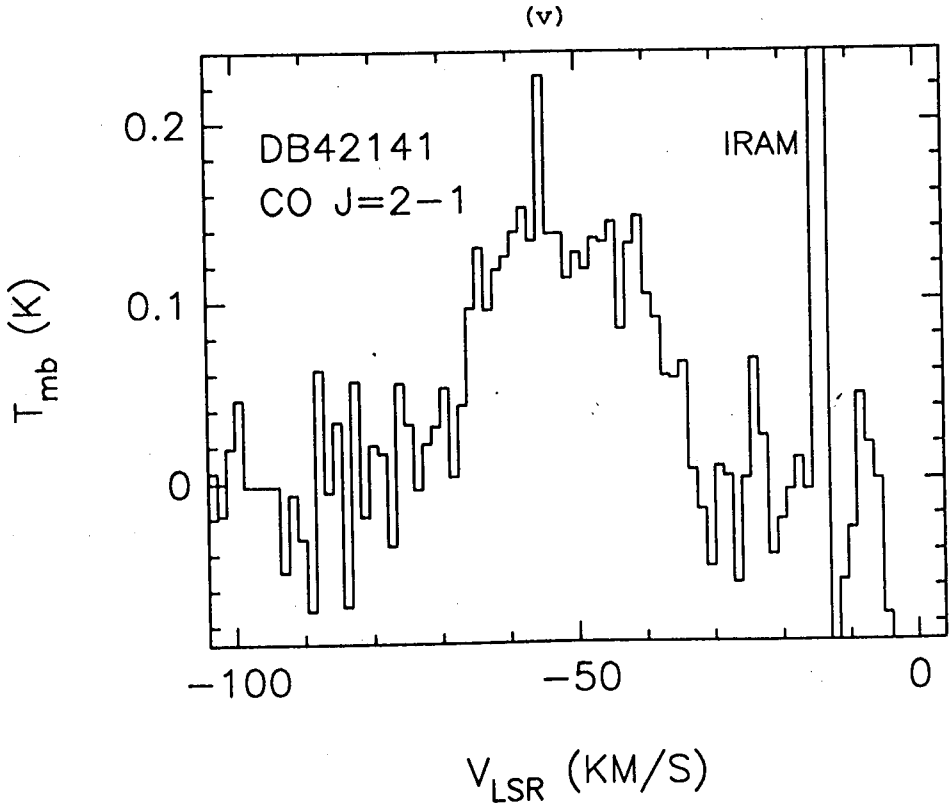
(v)
DB42141
CO J=2−1
IRAM
0.2
0.1
0
T_{mb} (K)
−100
−50
0
V_{LSR} (KM/S)

Fig. 1.

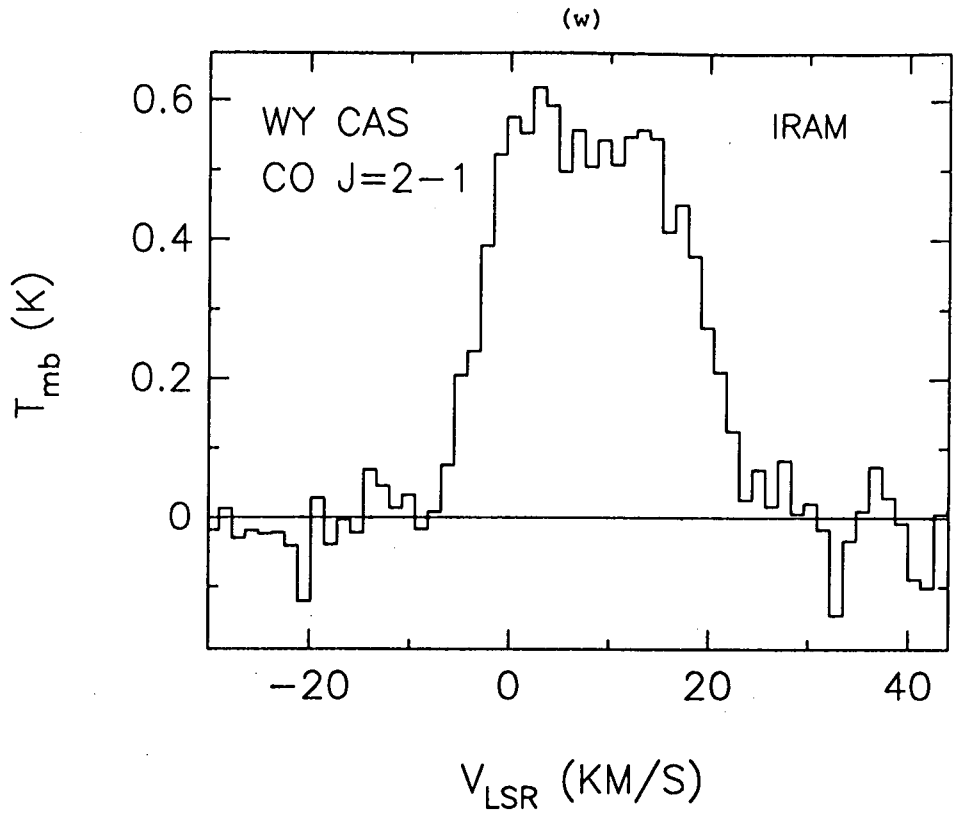
(w)
WY CAS
CO J=2−1
IRAM
0.6
0.4
0.2
0
T_{mb} (K)
−20
0
20
40
V_{LSR} (KM/S)

Fig. 2

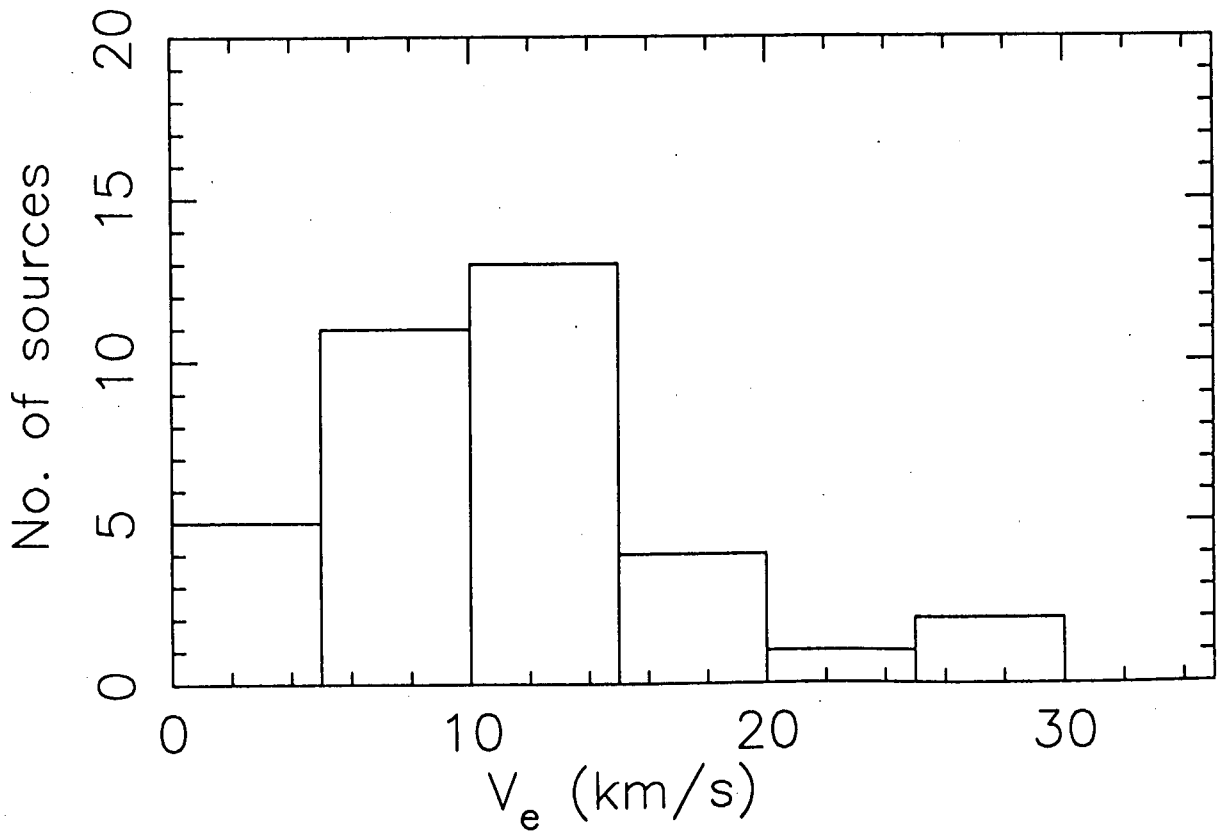
No. of sources
0
5
10
15
20
0
10
20
30
V_e (km/s)

Fig. 3 (a)

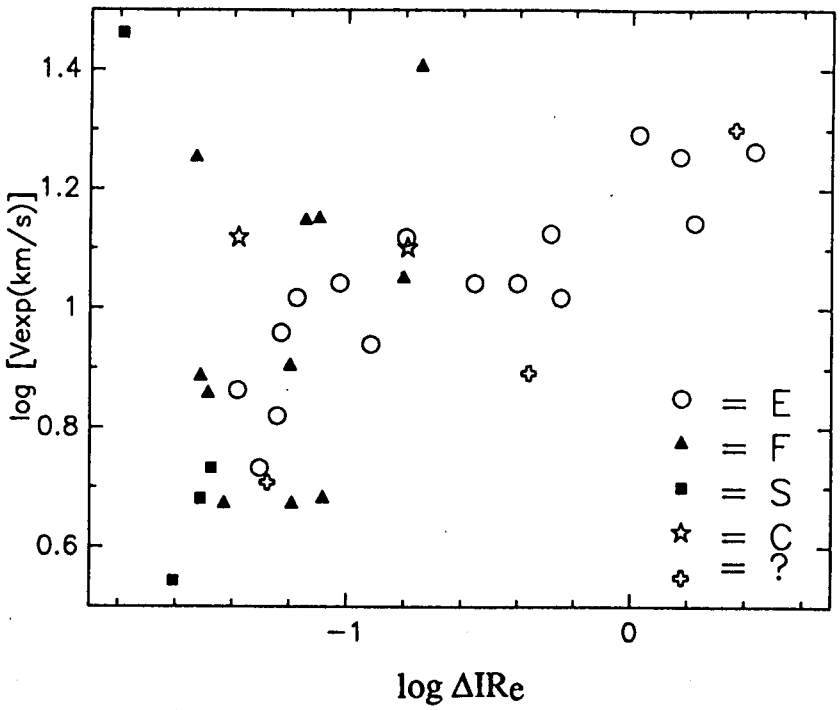
1.4
1.2
1
0.8
0.6
log [Vexp(km/s)]
−1
0
log ΔIRe
○ = E
▲ = F
■ = S
☆ = C
✣ = ?

Fig. 3(b)

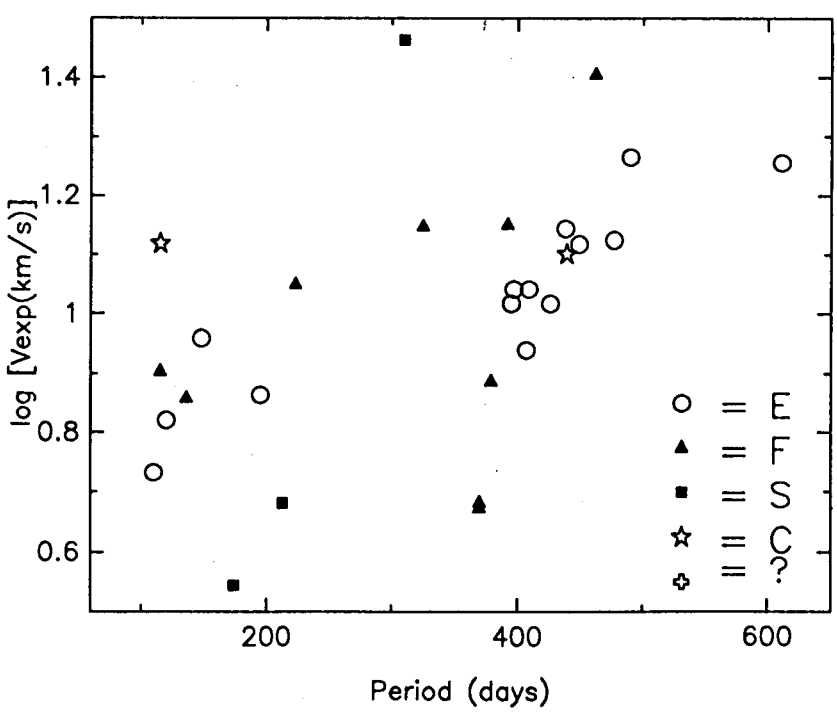
1.4
1.2
1
0.8
0.6
log [Vexp(km/s)]
200
400
600
Period (days)
○ = E
▲ = F
■ = S
☆ = C
✣ = ?

Fig. 4(a)

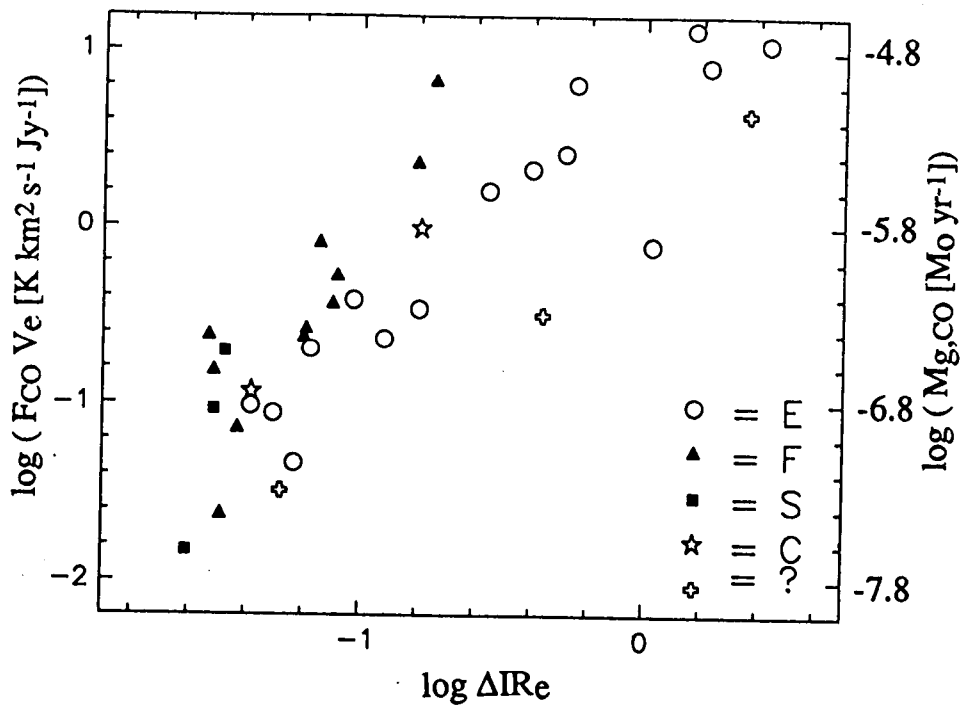
log (FCO Ve [K km2 s-1 Jy-1])
log (Mg,CO [Mo yr-1])
log ΔIRe
1
0
−1
−2
−1
0
-4.8
-5.8
-6.8
-7.8
O = E
▲ = F
■ = S
☆ = C
✣ = ?

Fig 4(b)

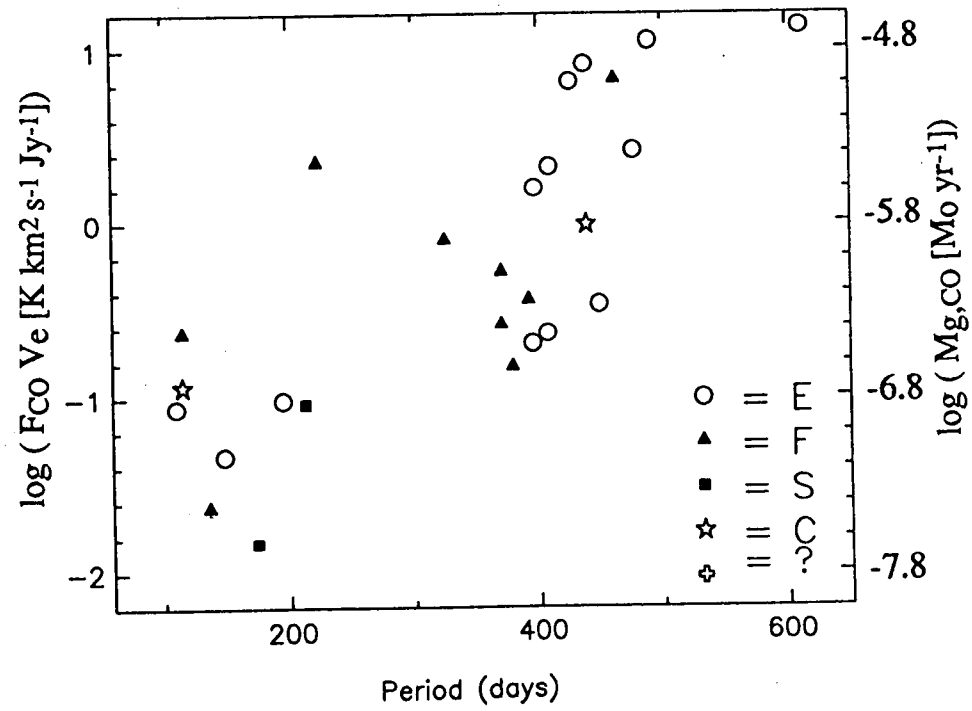
log (FCO Ve [K km2 s-1 Jy-1])
log (Mg,CO [Mo yr-1])
Period (days)
1
0
−1
−2
200
400
600
-4.8
-5.8
-6.8
-7.8
O = E
▲ = F
■ = S
☆ = C
✣ = ?